is equal to that of two singles ($2\rho_v = \rho_{2v}$). We found that $B_2 = 0.07 \pm 0.03$ eV and $B_3{}^d = 0.3 \pm 0.1$ eV. The binding energy of a divacancy is even somewhat smaller than before but is still within the assigned uncertainty of the previous analysis. The value of $B_3{}^d$ is not inconsistent with our estimates given above.

VIII. CONCLUSION AND SUMMARY

In summary, the best available values for the energies of formation and motion of vacancies and divacancies in gold are $E_M{}^1 = 0.82 \pm 0.03$ eV, $E_F{}^1 = 0.96 \pm 0.04$ eV, $E_M{}^2 = 0.66 \pm 0.06$ eV, $B_2 = 0.10 \pm 0.03$ eV, $B_3 \leq 0.3$ eV, and $B_3\theta \leq 0.2$ eV. In addition, if only single vacancies and divancicies are present and if they are in thermal equilibrium, then the diffusion of voids can be described using an effective diffusion constant. The effective diffusion constant expresses the fact that each vacancy during its random walk spends part of its lifetime as a single vacancy and part of its lifetime as a divacancy.

In conclusion, we like to compare our results on Au with the behavior of vacancies in quenched Ag. The life history of the defects in the two noble metals is completely different, mainly because of the large difference in binding energy for the divacancy. For Au, we measured $B_2 \cong 0.10$ eV, for Ag, Doyama and Koehler[9] reported $B_2 \sim 0.38$ eV. Therefore, in Au both singles and divacancies are present in the vicinity of room temperature. The defects anneal out by diffusing part of their lifetime as singles and the remainder as a member of a divacancy. The measured energy of migration E_m for this process is not a constant but depends on temperature and concentration of defects as observed. The minimum value of E_m is $E_m{}^2 - B_2 (\sim 0.55$ eV), and not the energy of migration for divacancies $E_m{}^2$. In Ag, on the other hand, the binding energy for divacancies is so large that all the quenched-in defects will be combined into pairs, and the energy of migration which one measures below room temperature is $E_m{}^2 (\sim 0.57$ eV).

ACKNOWLEDGMENTS

One of us (M. de Jong) wishes to express his sincere thanks to Professor D. Lazarus for stimulating this work, and to the Organization of European Economic Cooperation (O.E.E.C.) for receiving a travel grant which was obtained by the courtesy of the Netherlands Organization for the Advancement of Pure Research (Z.W.O.).

PHYSICAL REVIEW VOLUME 129, NUMBER 1 1 JANUARY 1963

Annealing of Pure Gold Quenched from above 800°C†

M. DE JONG* AND J. S. KOEHLER
Department of Physics, University of Illinois, Urbana, Illinois
(Received 6 August 1962)

The decrease of quenched-in resistivity as a function of time of Au wires quenched from above 800°C and then annealed in the vicinity of room temperature, is observed to be an S-shaped curve. The time $t_{1/2}$ required for half of the initially quenched-in resistivity ρ_0 to anneal out decreases from 15 to 0.5 h as quenching temperature is raised from 840 to 1000°C. It is observed that $1/t_{1/2} \propto \rho_0{}^{(2.60 \pm 0.2)}$. The fraction of ρ_0 that remains after infinite annealing times is independent of the quenching temperature with $\rho_r(\infty)/\rho_0 = 0.074 \pm 0.006$. All the S-shape annealing data combine into one universal curve if $f = [\rho - \rho_r(\infty)]/[\rho_0 - \rho_r(\infty)]$ is plotted against the reduced time $t/t_{1/2}$. The universality of the curves indicates that the supersaturated concentrations of defects in Au disappear by one unique process. The following process is proposed: The defects in freshly quenched specimens are present as single vacancies, divacancies, and trivacancies, which are in thermal equilibrium with one another. The concentration of other complexes is negligible. Tetrahedra of stacking faults, as observed by Hirsch, act as the sinks for singles and divacancies. They are formed during annealing by the collapse of six aggregated vacancies; their nucleation sites are the tetravacancy complexes, which are the smallest vacancy clusters in Au which are not in thermal equilibrium. The tetravacancy converts into a tetrahedron if struck by a divacancy. The remaining resistivity is due to the stacking faults of the tetrahedra. If it is assumed, in addition, that all the quenched-in defects disappear at the tetrahedra, then $\rho_r(\infty)/\rho_0$ is shown to be a constant as observed and the parameter f then represents the fraction of the initially quenched-in defects that has not yet been absorbed. The model predicts that $1/t_{1/2} \propto c_0{}^{2.5}$ and that the number of tetrahedron n_∞ at infinite annealing times is $n_\infty \propto c_0{}^{1.5}$ in agreement with the experiments. The resistivity of stacking faults per unit area was calculated to be $(1.3 \pm 0.4) \times 10^{-13}$ Ωcm².

I. INTRODUCTION

IT was observed by Bauerle and Koehler[1] that if Au wires are quenched from above 800°C and subsequently annealed in the vicinity of room temperature, the annealing curve is not essentially exponential, but has an S shape (Fig. 1). The time required for half of the resistance increment to anneal decreases as the quenching temperature is raised. In addition, about 7% of the quenched-in resistivity cannot be annealed out in the neighborhood of room temperature.

The data for quenches from various high temperatures can all be plotted on one graph if f, the fraction

† Research supported by the Office of Naval Research and the U. S. Atomic Energy Commission.
* Present address: Natuurkundig Laboratorium, University of Amsterdam, The Netherlands.
[1] J. E. Bauerle and J. S. Koehler, Phys. Rev. **107**, 1493 (1957).

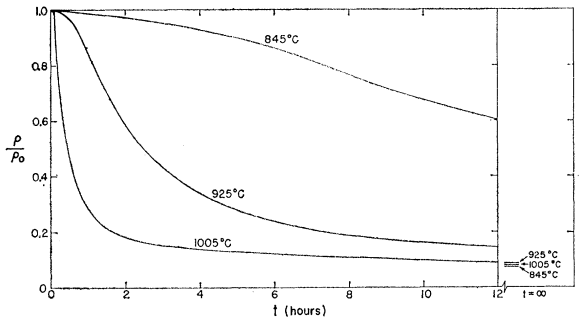

FIG. 1. The relative decrease of resistivity, ρ/ρ_0, as a function of time for three Au wires, quenched from 845, 925, and 1005°C, respectively, and annealed at 40.15°C.

of the resistivity increment remaining at time t, is plotted against a reduced time τ. Suppose the resistivity is measured at 4.2°K for a pure specimen. In this case, only vacancies and vacancy clusters contribute to the resistivity. Then f is defined as

$$f=[\rho-\rho_r(\infty)]/[\rho_0-\rho_r(\infty)], \quad (1)$$

where ρ is the resistivity at time t, ρ_0 is the initial quenched-in resistivity, and $\rho_r(\infty)$ is the resistivity after infinite annealing time. The reduced time τ is $t/t_{1/2}$, where $t_{1/2}$ is the time required for f to drop to one-half. The extent to which the data fit this universal plot is shown in Fig. 2. The fact that all high-temperature curves have the same shape each characterized by just one time constant indicates that a single basic process is responsible. In this paper, an attempt will be made to gain some insight into this process.

Koehler, Seitz, and Bauerle[2] suggested that the S-shape curve arises from the clustering of vacancies producing new sinks. Subsequently, Silcox and Hirsch,[3] and later Cotterill,[4] observed tetrahedra in gold specimens quenched from 850°C and above and then annealed at 100°C. The tetrahedra were observed by transmission electron microscopy. They were not present immediately after quenching. Their development during annealing has not been followed. The faces of the tetrahedra are stacking faults; their edges are partial dislocations; their size ranges from 270 to 580 Å in Cotterill's observations.

Cotterill also observed that the remaining resistivity $\rho_r(\infty)$ is directly related to these tetrahedra. It is clear that if one attempts to describe the universal S-shaped curve in some detail one has to determine how and when the new sinks are formed and how they can absorb vacancies. These questions will be discussed in the following sections.

Kimura *et al.*[5] have made an attempt to explain the S-shaped curve using a specific model for the sinks. They assumed that the new sinks are sessile dislocation rings on (111) planes formed by the aggregation and condensation of vacancies, and that nucleation is accomplished for the most part *during* quenching. The periphery of the sessile dislocation grows as annealing proceeds, thus continuously increasing the number of absorption sites. In order to fit this model to Bauerle's data, and in order to explain that new dislocation rings are only formed during quenches from above 750°C and not from below, where no S-shaped curve was found, they made some additional *ad hoc* assumptions.

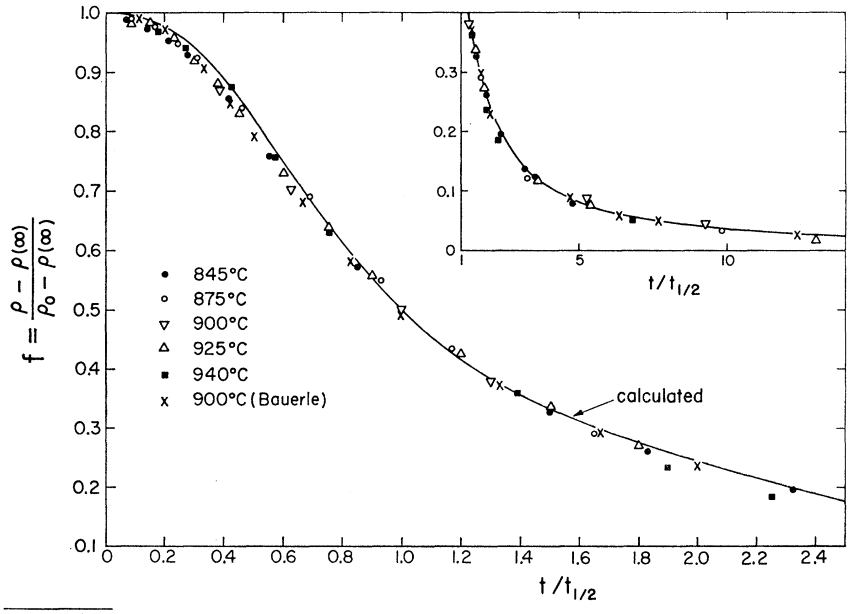

FIG. 2. $f=[\rho-\rho(\infty)]/[\rho_0-\rho(\infty)]$ as a function of $t/t_{1/2}$ of Au wires, quenched from various temperatures in the range of 845–950°C, and annealed at 40°C. The full line is the calculated curve for a model presented in Sec. VI.

[2] J. S. Koehler, F. Seitz, and J. E. Bauerle, Phys. Rev. **107**, 1499 (1957).
[3] J. Silcox and P. B. Hirsch, Phil. Mag. **4**, 72 (1959).
[4] R. M. J. Cotterill, Phil. Mag. **6**, 1351 (1961).
[5] H. Kimura, R. Maddin, and D. Kuhlmann-Wilsdorf, Acta Met. **7**, 145 (1959).

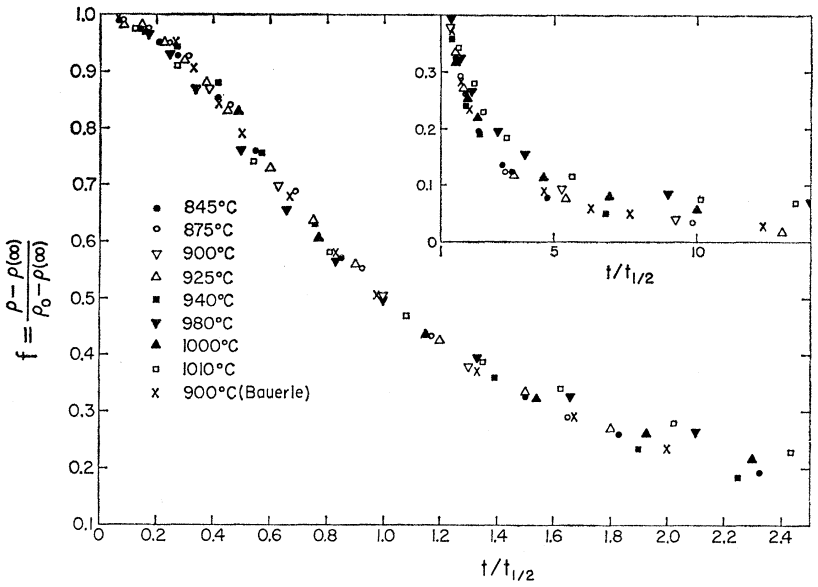

FIG. 3. f as a function of $t/t_{\frac{1}{2}}$ of Au wires quenched from above 800°C and annealed at 40°C.

Besides the normal attractive binding energy of a divacancy (they choose $B_2=0.40$ eV), they postulated a repulsive energy ($\sim$0.24 eV) dominating at small distances. Due to this repulsion, no clustering during quenching was supposed to occur at low vacancy concentrations. Moreover, singles and divacancies will no longer be in chemical equilibrium but singles will anneal out as singles and divacancies as divacancies. In addition, they had an adjustable parameter which results from the fact that the stable dislocation network and the sessile rings act as sinks concurrently. In the previous paper (to be referred to as I), it is shown that their complicated picture for the binding energy of a divacancy does not fit the experimental annealing data, and that by treating the singles and divacancies as being in thermal equilibrium, one can understand in a very satisfactory way the continuous range of energies of migration. In the next sections, additional experimental phenomena will be described and examined which do not fit with their model.

II. EXPERIMENTAL RESULTS

Figure 1 shows the relative decrease in resistivity ρ/ρ_0 as a function of time for three Au specimens quenched from different temperatures (845, 925, and 1005°C), and annealed at 40.15±0.02°C. The time $t_{1/2}$ required for half the resistivity increment to anneal out, decreases from 15 to 0.5 h as the quenching temperature increases from 845 to 1000°C. In addition, about 7% of the initial resistivity cannot be annealed out in the vicinity of room temperature. The resistivity at infinite annealing times, $\rho_r(\infty)$, was determined by finally annealing the wires for 5 min at 350°C, which procedure will be justified below (Fig. 4). In Fig. 3 all the curves obtained for quenches from above 800°C are plotted using the reduced scales f and $t/t_{1/2}$, where f is defined by Eq. (1). It can be seen that for quenches in the range of 845–950°C the resulting curves nicely combine into one universal S-shaped curve, as also shown in Fig. 2. We may note that for quenches from around 1000°C deviations of this universality appear especially at long times. It looks as though the resistivity at infinite annealing times $\rho_r(\infty)$ obtained by the procedure mentioned above does not represent the proper value to be used for the latter decay curves.

In order to decide whether other stable vacancy complexes besides singles, divacancies, and tetrahedra are formed during the annealing process, an isochronal annealing curve was determined using a wire quenched from 1000°C and subsequently pre-annealed for 3 h at 40°C (i.e., about 11 times the half-time). Two recovery steps were found (Fig. 4), at 80 and 600°C, respectively. Essentially the same result was obtained for a wire quenched from 900°C and pre-annealed for 33 h at 40°C (i.e., 10 times the half-time).

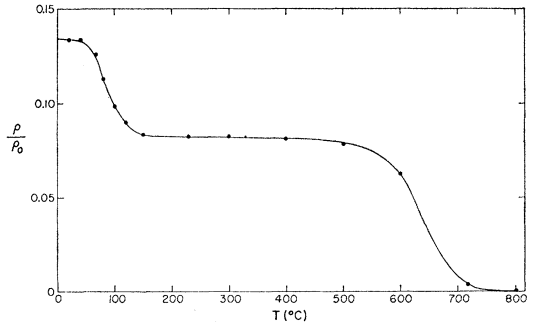

FIG. 4. Isochronal annealing curve of a wire quenched from 1000°C and subsequently pre-annealed for 3 h at 40°C (i.e., about 11 times the half-time). The specimen was held at each temperature for 10 min.

Kimura *et al.*[5] assumed that what they call "the nuclei for sinks" are formed for the most part *during* quenching. On the other hand, Cotterill[4] did not observe tetrahedra in freshly quenched gold foils, but found 25 Å black spots which were not resolved. As yet it is not clear what the black spots are. In addition, we may note that he lost an appreciable fraction of the defects during quenching, especially from high temperatures (see Fig. 3 of Simmons and Balluffi's paper[6]). Some of these vacancies may have formed small clusters. In order to check this point, a wire was quenched from 900°C and subsequently annealed for 10 min at 400°C. More than 99.7% of the initially quenched-in resistivity annealed out. This indicates that the concentration of large sinks (i.e., of large tetrahedra) present directly after quenching is negligibly small, in agreement with Cotterill's observation. It is, of course, possible that small sized sinks may break up at some temperature below 400°C.

III. VACANCY COMPLEXES

In order to gain some insight into the formation of sinks by the clustering of vacancies, we now would like to discuss the tri- and tetra-vacancy. The matter is sufficiently complex to make detailed description difficult. The experimental information is scarce and the theoretical investigations have lead to such diverse conclusions that we were left without much guidance. We will, therefore, restrict ourselves to those aspects which are relevant to their role as links in the chain of vacancy clusters. The topics to be considered are: (1) The various kinds of trivacancies and their kinetics, (2) the question of whether trivacancies are in thermal equilibrium with singles and divacancies, and (3) the formation of the tetravacancy.

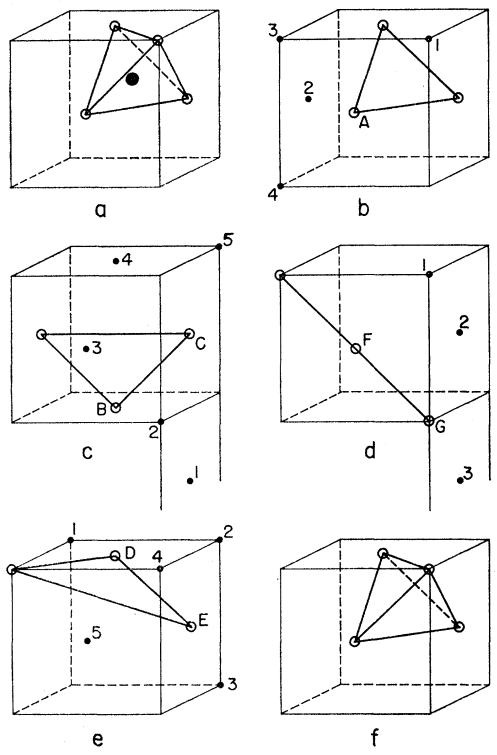

FIG. 5. (a)–(e) Five different configurations of trivacancies. (f) The tetravacancy of the tetragonal form. The letters and numbers refer to the various dissociation processes listed in Table I.

First, however, we would like to analyze the isochronal annealing curve given in Fig. 4, which deals with vacancy complexes in gold in general. Recovery steps were found at 80 and 600°C. Cotterill[4] showed that the latter step is due to the dissolution of tetrahedra; a conclusion arrived at by comparing the remaining resistivity of foils quenched from 850°C and annealed at 100°C with electron microscope pictures, taken from the same foil. The step at 80°C represents the annealing out of singles and divacancies. The average time t it takes these defects to reach the sinks is: $t=X^2/2D_{\text{eff}}$, where D_{eff} is given by Eq. (3) of paper I and $2X$ is the average spacing between sinks. Substituting the appropriate numbers ($X=\frac{1}{2}\times10^{-5}$ cm, $E_m{}^1=0.82$ eV, $E_m{}^2-B_2=0.56$ eV, $c_1=4\times10^{-5}$, and $T=353$°K) gives $t=17$ min, which compares well with the experimental annealing times of 10 min.

Since no other recovery steps are found, one has three alternatives for the larger vacancy complexes:

(a) Besides singles and divacancies on the one hand, and the tetrahedra on the other, all other complexes contribute less than 0.1% to the initially quenched-in resistivity so that they escape detection.

(b) The complexes are so stable that they decompose together with the tetrahedra.

(c) Their lifetime τ is considerably less than 10 min at 80°C (the time it takes the decomposition products to reach the sinks has to be included). In general, τ is given by $1/\tau=\nu e^{-(E_m+B)/kT}$, where E_m is the energy of migration of the breakaway defect and B the binding energy of the cluster; ν is the frequency factor and contains a geometrical factor. Assuming $\tau=2$ min and $\nu=10^{13}$ per sec, one finds for these clusters the condition: $E_m+B\leq1.05$ eV. Thus, if the breakaway defect is a single vacancy, $B\leq0.23$ eV and if it is a divacancy, $B\leq0.4$ eV.

A. The Trivacancy

There are five different configurations of trivacancies indicated in Fig. 5. The triangular configuration in the (111) plane (denoted by t^{60}) and the tetragonal form with one atom inside the tetrahedron as suggested by Dienes and Damask[7] [Figs. 5(a) and (b)] involve close-packed vacancies. Theoretical estimates made by Dienes and Damask[7] and by Vineyard[8] for copper both

[6] R. O. Simmons and R. W. Balluffi, Phys. Rev. **125**, 862 (1962).

[7] A. C. Damask, G. J. Dienes, and V. G. Weizer, Phys. Rev. **113**, 781 (1959).

[8] G. H. Vineyard, Disc. Faraday Soc. **32**, 7 (1962).

suggest that the tetrahedral configuration has lowest energy. Dienes *et al.* found a binding energy of 1 eV, whereas Vineyard found 0.46 eV.

The isochronal annealing curve described above, plus additional calculations which we now describe, show that the binding energy of a trivacancy in gold is probably less than 0.4 eV. Let us consider this matter in more detail. From the discussion of the isochronal annealing from 80 to 600°C given above, the binding energy of a trivacancy, whatever its configuration, must either be less than 0.4 eV or it must be greater than 1.9 eV if the trivacancy does not break up in the range from 80 to 600°C. If $B_3>1.9$ eV, then the trivacancies do not come into equilibrium during the annealing after a quench from above 800°C. In this case, the trivacancies act as sinks for vacancies and subsequently grow into tetrahedra by the absorption of additional vacancies. This model has been used; it gives an S-shaped curve, but three discrepancies with the experimental result (see Sec. V). The size of the final tetrahedra, the dependence of the half-time, and the concentration of tetrahedra on the initial vacancy concentration are all in error. The trivacancy breakup should produce a change in resistivity which is large enough to be observable if B_3 is in the range between 0.4 and 1.9 eV. For example, if $B_3=0.46$ eV and if the trivacancies are in equilibrium with single vacancies and divacancies then the trivacancies contribute about 5% to ρ_0 (see Paper I). The trivacancy contribution would be even larger if they are not in equilibrium (Sec. VI). Therefore, since no annealing step in the isochronal is observed, and since a poor fit to the S-shaped curve is obtained using trivacancies as cluster nuclei, we conclude $B_3\leq 0.4$ eV and that the trivacancies are present in thermal equilibrium with single vacancies and divacancies during most of the anneal.

There is one remaining question, i.e., what is the stable trivacancy configuration in gold? We assume that it is the triangular configuration t^{60} in the (111) plane. It could of course be the tetrahedral configuration. The lattice can go from the t^{60} configuration to the tetrahedral configuration by allowing a single atom to fall into the center of the tetrahedron. If the tetrahedral trivacancy configuration is stable then our kinetic equations have omitted this relaxation. Therefore the results would not be altered in a very important way if the tetrahedral trivacancy is to be preferred. If so, the frequency factors associated with the formation and breakup of trivacancies would probably be smaller than if the triangular trivacancy is the stable unit.

The other trivacancy configurations are less compactly stacked; they enclose angles of 90°, 120° and 180°, respectively [Fig. 5(c), (e), (d)]. They are denoted by t^{90}, t^{120}, t^{180}.

The formation and dissociation processes for trivacancies are given in Table I and Fig. 5. The migrating defect can be either a single vacancy or a divacancy (last column). In the case of dissociation, the migrating defect is considered to be a single vacancy if the breakaway defect becomes separated from the initial complex as a single [$A\rightarrow 4$ in Fig. 5(b)]; in all other cases the dissociation is assumed to involve a divacancy motion (e.g., $A\rightarrow 2$ or $D\rightarrow 2$). A similar assumption was made for the reverse process, the formation of trivacancies. Examination of Table I reveals that the stable trivacancy t^{60} cannot dissociate by the motion of a divacancy into two well separated entities, i.e., a single and a divacancy. This means, vice versa, that by the encounter of a single vacancy and the faster moving divacancy, a noncompact trivacancy must be formed rather than the t^{60}. Therefore, the t^{90} and t^{120} are important as intermediate steps in the formation of the t^{60}. In addition we may note that the t^{180} is of nearly no importance in the chain of vacancy clusters and it is neglected from now on.

TABLE I. Dissociation of trivacancies.

Initial configuration	Final configuration	Example (see Fig. 5)	Total No. of equivalent jumps	Moving defect[a]
60° trivacancy [Fig. 5(b)]	60°	$A\rightarrow 1$	3	
	90°	$A\rightarrow 2$	6	d
	120°	$A\rightarrow 3$	6	d
	single & div.	$A\rightarrow 4$	15	s
		total	30	
90° trivacancy	3 singles	$B\rightarrow 1$	4	s
[Fig. 5(c)]	1 single & div.	$B\rightarrow 2$	4	d
		$C\rightarrow 5$	12	s
	90°	$B\rightarrow 3$	2	d
		$C\rightarrow 4$	2	s
	120°	$C\rightarrow 2$	4	d
	180°			
	60°	$C\rightarrow 3$	4	d
		total	32	
120° trivacancy	3 singles	$D\rightarrow 1$	3	s
[Fig. 5(e)]	1 single & div.	$E\rightarrow 3$	14	s
		$D\rightarrow 2$	6	d
	90°	$E\rightarrow 4$	2	d
	120°	$D\rightarrow 5$	3	d
	180°	$E\rightarrow 2$	2	d
	60°	$E\rightarrow 5$	2	d
		total	32	
180° trivacancy	3 singles	$F\rightarrow 1$	2	s
[Fig. 5(d)]	1 single & div.	$G\rightarrow 3$	14	s
		$F\rightarrow 2$	8	d
	120°	$G\rightarrow 2$	8	d
		total	32	

[a] s = single vacancy; d = divacancy.

Table I enables us to write down the differential equations which govern the concentrations of trivacancies, c_3^{60}, c_3^{90}, c_3^{120}, and c_3^{180}. They are given in the Eqs. (1c–f) of Paper I. A scheme of the energy barriers used between the various configurations is given in Fig. 6. It is assumed here that if the migrating defect is a single vacancy, E_m^1 and ν_1 are the proper energy of migration and the frequency factor; likewise E_m^2 and

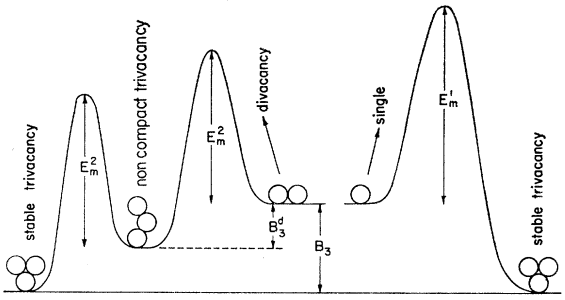

FIG. 6. Scheme of the energy levels used in the kinetic equations for the trivacancies (Eq. 1 of paper I).

ν_2 were used in the case of the divacancy. This tends to overestimate the energies of migration involved, e.g., the jump $C \rightarrow 3$ will likely involve an energy less than E_m^2.

For the case that trivacancies are in thermal equilibrium with singles and divacancies, their concentrations can be derived from Eq. (1) of Paper I. They are

$$\begin{aligned} c_3 &= 8c_1^3 e^{(B_3+B_2)/kT}, \\ c_3^{90} &= 12c_1^3 e^{(B_3{}^d+B_2)/kT}, \\ c_3^{120} &= 24c_1^3 e^{(B_3{}^d+B_2)/kT}. \end{aligned} \tag{2}$$

Here we assumed that $B_3{}^{90}=B_3{}^{120}=B_3{}^d$ and used the simplified notation: $B_3{}^{60}=B_3$ and $c_3{}^{60}=c_3$. B_3 and $B_3{}^d$ are the energy increases which occur when a trivacancy t^{60} and a noncompact trivacancy, respectively, are broken into a single vacancy and a divacancy.

The formation and dissociation processes, which involve the motion of a divacancy, strongly over those involving a single vacancy, because for Au $E_m{}^2 \ll E_m{}^1$; e.g., in the Eqs. (1) of Paper I, $\gamma_1 \ll \delta_1$ and $\gamma_2 \ll \delta_2$. Therefore, the average time τ_3 required for a noncompact trivacancy to break up is given by

$$1/\tau_3 = \gamma_2 (= 4\nu_2 e^{-(E_m{}^2+B_3{}^d)/kT}),$$

and likewise the time τ_3' required for the dissociation of a t^{60} into a noncompact trivacancy is

$$1/\tau_3' = \pi_2 (= 6\nu_2 e^{-(E_m{}^2+B_3-B_3{}^d)/kT}).$$

Because one can expect that $B_3 - B_3{}^d \lesssim B_3{}^d$, it follows that $\tau_3 \gtrsim \tau_3'$.

Equilibrium between singles, di-, and tri-vacancies is achieved, if the average time τ required to establish equilibrium is much smaller than the average time it takes the singles and divacancies to reach the sinks. Hence $\tau \ll X^2/2D_{\text{eff}}$. In the most unfavorable situation τ is given by $\tau = \tau_3$. Substitution of $X = \frac{1}{2} \times 10^{-5}$ cm, $c_0 = 3 \times 10^{-4}$, which corresponds to a 1000°C quench, and $B_2 = 0.1$ eV, one finds that thermal equilibrium is maintained if $B_3{}^d < 0.55$ eV. This condition is very likely to be fulfilled because if $B_3{}^d \geq 0.4$ eV nearly all the defects are combined into trivacancies (see Paper I) so that they should have appeared as a separate step in the isochronal annealing curve (Fig. 4). In addition it was shown in Paper I that B_3 is likely to be less than 0.3 eV.

B. The Tetravacancy

The total number of various tetravacancies one can think of is even larger than the number of trivacancies. Some configurations of four vacancies were investigated theoretically by Vineyard.[8] Here only the tetravacancy of the tetragonal form will be considered [Fig. 5(f)], even though this is unstable according to Vineyard's calculation. The tetravacancy can be formed by the encounter either of a single vacancy with a trivacancy, or of a divacancy with another divacancy. The differential equation which describes these processes is given in Eq. (1g) of paper I. We now show that in gold the di-di encounter can be neglected. The probability for this process is given by the condition that the average lifetime τ_2 of the divacancy is longer than the time τ_2' it takes a divacancy to encounter another divacancy, $\tau_2 > \tau_2'$. $1/\tau_2 = \alpha_2$ and $1/\tau_2' = \xi_1 c_2$. Hence,

$$\frac{1}{c_1{}^2} < \frac{6\xi_{10}}{14} \frac{\nu_2}{\nu_1} e^{+(E_m{}^1 - E_m{}^2 + 2B_2)/kT}. \tag{3}$$

ξ_{10} is a geometrical factor which depends on the various kinds of other tetravacancies one wants to incorporate. Usually, $\xi_{10} \sim 25$. Substituting $\nu_2/\nu_1 = 1/3$, $E_m{}^1 + B_2 - E_m{}^2 = 0.26$ eV, and $B_2 = 0.10$ eV one obtains for 40°C: $c_1 > 7 \times 10^{-4}$. This can never be achieved in a quenching experiment in gold. On the other hand at 0°C one finds for the critical single-vacancy concentration: $c_1 > 2.2 \times 10^{-4}$, so that at this annealing temperature a small contribution from di-di encounters can be expected for specimens quenched from about 1000°C. If the above numbers are used except that $B_2 = 0.13$ eV then the critical concentrations for single vacancies, divacancies (in equilibrium), and total vacancies at 40°C are: $c_1 = 2.8 \times 10^{-4}$, $c_2 = 0.59 \times 10^{-4}$, and $c_1 + 2c_2 = 3.98 \times 10^{-4}$. At 0°C the critical concentrations are: $c_1 = 9.3 \times 10^{-5}$, $c_2 = 1.3 \times 10^{-5}$, $c_1 + 2c_2 = 1.06 \times 10^{-4}$. The maximum total vacancy concentration quenched in from 1000°C is 3.3×10^{-4}. Hence, even if $B_2 = 0.13$ eV, the di-di encounters do not dominate at 40°C, although they would influence matters if the annealing is done at 0°C. We may note the marked difference in the role of the di-di encounter in Au when compared with the same process in Ag. Doyama and Koehler[9] showed that in the latter noble metal this process is very important and dominates during annealing below 0°C.

The stable form and the binding energy of the tetravacancy are not well known. Vineyard[8] estimated the binding energy to be about 0.7 eV in copper relative to four well separated single vacancies. We assume that the form is the tetrahedron and that the tetravacancy is sufficiently stable so that on the average further

[9] M. Doyama and J. S. Koehler, Phys. Rev. **127**, 21 (1962).

vacancies join the tetravacancy before it breaks up. The stable form may not be the tetrahedral form, but this should only alter the frequency factors used in the present treatment. Thus, we assume that the tetravacancy is the smallest vacancy cluster in gold, which is no longer in thermal equilibrium with singles and divacancies. The assumption that the tetravacancy is not present in thermal equilibrium and thus that it constitutes the nucleous for the large observed tetrahedra gives annealing kinetics which fit the observed results (see below). It is of course possible that the tetravacancy binding energy is small and that a larger cluster is required to nucleate the large tetrahedra.

IV. THE TETRAHEDRON

Silcox and Hirsch,[3] and later Cotterill,[4] showed that in gold the aggregated vacancies form tetrahedra; the faces are stacking faults along (111) planes, the edges are stairrod dislocations along [110] directions. Hirsch *et al.*[3] and Kühlmann-Wilsdorf[10] proposed that the tetrahedra are formed by the dissociation of a sessile ring dislocation into partials. The sessile ring was then supposed to result from the collapse of aggregated disk of vacancies in the (111) planes. The existence of these plates and loops in quenched gold is doubtful because (1) they have not been observed by electron microscopy in quenched and annealed Au; (2) their existence is not indicated by our isochronal annealing curve (Fig. 4); one should expect them to produce a separate recovery step; and (3) energy considerations indicate an upper limit for the size of the tetrahedra but no lower limit.[3] This suggests that the sinks formed by the clustering of vacancies during annealing of quenched Au might have the tetrahedral configuration from the early beginning, and that no intermediate stages exist.

One is led to ask what is the smallest tetrahedron of stacking faults one can form and how can it act as a sink. The smallest one is the tetrahedral trivacancy proposed by Dienes and Damask[7] [Fig. 5(a)]. It consists of only one incorrectly stacked atom. It is doubtful whether it makes sense to consider its bounding faces as planes of stacking faults. The next larger size can be formed by the collapse of six vacancies. Here four atoms are stacked out of order. The creation of this tetrahedron involves the disappearance of the six originally clustered vacancies. We may note that we deal here with the first process in which vacancies are annihilated by means other than the climb of dislocations. In addition since an aggregate of six vacancies collapses into a tetrahedron, the tetra- and pentavacancy appear to be the largest stable complexes of vacancies in gold.

There are various processes which lead to the creation of the tetrahedron:

(1) By the simultaneous encounter of three vacancies with a trivacancy. Because of the short lifetime of the trivacancy (Sec. III), this process is not very likely.

(2) By the encounter of a divacancy with a tetravacancy, or of a single vacancy with a pentavacancy. Both processes seem conceivable and both therefore, are considered in our final model for the *S*-shaped curve (Sec. VI).

The tetrahedron can absorb vacancies at its edges. This mechanism is elucidated by using the cork model pictured in Fig. 7. The black balls represent the tetrahedron, the white ones form part of the regular f.c.c. lattice lying on (111) faces. The uncolored balls belong to the regular lattice and form part of the stairrod dislocation. Let us assume a vacancy A has diffused into them. This vacancy can now be absorbed by displacing the whole row of uncolored balls over through $(a/6)[112]$ resulting in Fig. 7(b). So the annihilation of one vacancy leads to an increase of the size of the tetrahedron by a whole row of atoms. Figures 7(c) and (d) give a schematic representation of the tetrahedron before and after the annihilation of the vacancy. It is clear that each time a vacancy becomes attached to one of the stairrod dislocations it can be annihilated by the same process. We may note that the absorption of vacancies at the corners of the tetrahedra can be accomplished by essentially the same rearrangement of atoms.

It can be shown that vacancy absorption at the faces

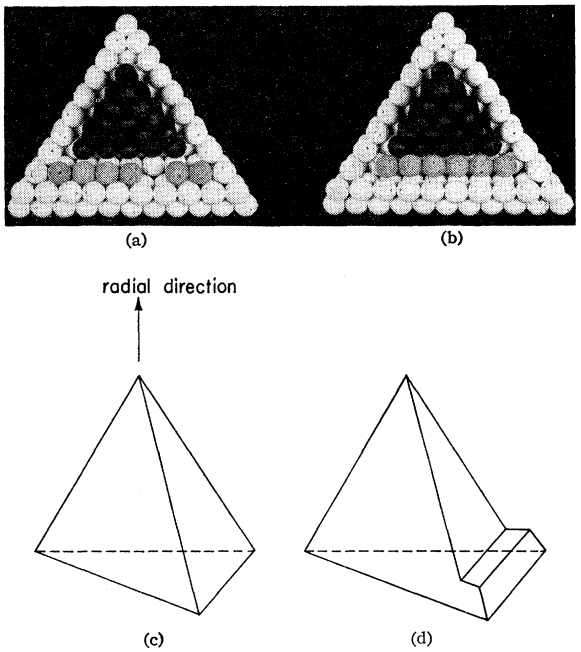

FIG. 7. (a) and (b) Configuration of the atoms adjacent to the edge of a tetrahedron (black balls), before and after absorption of a vacancy (missing atom in the uncolored row of cork balls). (c) and (d) Schematic drawing of the shape of the tetrahedron before and after absorption of a vacancy.

[10] D. Kuhlmann-Wilsdorf, R. D. Maddin, and H. Kimura, Z. Metallk. **49**, 584 (1959).

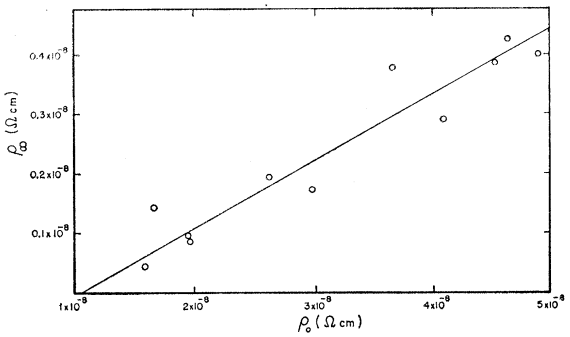

FIG. 8. The resistivity at infinite annealing times, $\rho_r(\infty)$, as a function of the initially quenched-in one, ρ_0.

instead of at the edges involves the *simultaneous* encounter of three vacancies at the surface of the tetrahedron, which is very unlikely.

Although the whole stairrod dislocation can act as a sink for vacancies, there are other factors which may influence the actual sites where a vacancy is trapped, e.g., by taking into account the interaction between the vacancy and the tetrahedron.[11] As is discussed in Appendix A, it is conceivable that the corners are the dominant absorption sites.

If the edges of the tetrahedra act as sinks, the number of sites per tetrahedron, m, is given by

$$m=[(c_0-c)N/n]^{1/2}m_0. \tag{4}$$

If the corners act as such, Eq. (4) reduces to $m=4$. Here, c_0-c is the total concentration of vacancies annealed out, N is the number of atoms per cc, m_0 is the number of stairrod dislocations per tetrahedron, thus $m_0\geq 6$ depending on the total number of steps per face [see Fig. 7(d)].

V. THE REMAINING RESISTIVITY

The annealing of quenched-in defects in Au wires is generally studied by measuring the electrical resistivity ρ at e.g., 4.2°K. In the case of quenches from above 800°C, ρ consists of two parts, namely, the resistivity of the vacancies and vacancy clusters, still present, ρ_m, and the resistivity of the tetrahedra, ρ_r. Hence,

$$\rho=\rho_m+\rho_r \tag{5a}$$

with

$$\rho_m=\rho_v(c_1+2c_2+3c_3+4c_4). \tag{5b}$$

Experiments have shown that probably no tetrahedra are present directly after quenching, thus giving the boundary condition $\rho_r=0$ at $t=0$. Here, it is assumed that the remaining resistivity is due to the tetrahedra formed during annealing as proved by Cotterill,[4] and that $\rho_v=\frac{1}{2}\rho_{2v}=\frac{1}{3}\rho_{3v}=\frac{1}{4}\rho_{4v}$ which seems reasonable in view of the results of Paper I. (ρ_v, ρ_{2v}, ρ_{3v}, and ρ_{4v} are the resistivities of 1 mole of single, di-, tri-, and tetravacancies.)

First, let us examine the remaining resistivity ρ_r. Let us assume that all the vacancies disappear at the tetrahedra (the annihilation of vacancies at the existing dislocations can be neglected as is shown in the next section), and that the remaining resistivity is solely due to the stacking faults of the tetrahedra[12]: Then the resistivity of n tetrahedra of average edge length L is

$$\rho_r=4n(\tfrac{1}{4}\sqrt{3}L^2)\rho_{S.F.}, \tag{6a}$$

where $\rho_{S.F.}$ is the resistivity per unit area of stacking fault.

The total number of vacancies n_v trapped by these tetrahedra is

$$n_v=nL^2/a^2, \tag{6b}$$

but this is also given by

$$n_v=N(\rho_0-\rho_m)/\rho_v, \tag{6c}$$

where a is the smallest distance between two atoms.

Combining (6a, b and c) gives

$$\rho_r=Na^2\sqrt{3}(\rho_0-\rho_m)\rho_{S.F.}/\rho_v. \tag{7}$$

For infinite annealing times one obtains

$$\rho_r(\infty)=Na^2\sqrt{3}(\rho_{S.F.}/\rho_v)\rho_0. \tag{8}$$

Equation (8) has certain important features. It shows that the resistivity at infinite annealing times $\rho_r(\infty)$ in the neighborhood of room temperature, is proportional to the initially quenched-in resistivity ρ_0. The experimental results plotted in Fig. 8 confirm this conclusion. The straight line is obtained by the least-square method, and gives $\rho_r(\infty)/\rho_0=0.074\pm0.006$.

Equation (8) also enables us to estimate $\rho_{S.F.}$. Using Simmons and Balluffi's value[6] for $\rho_v=(1.5\pm0.3)\times10^{-4}$ Ωcm, one finds $\rho_{S.F.}=(1.3\pm0.4)\times10^{-13}\Omega$ cm^2. This agrees within experimental error with Cotterill's value[4] of $[1.8\pm0.3]\times10^{-13}\Omega$ cm^2 obtained by measuring the resistivity after prolonged annealing at 100°C and counting the total area of stacking faults from electron microscopy pictures. Also fair agreement exists with the theoretical calculations of Howie,[12] who arrived at 2.5×10^{-13} Ωcm^2.

Next consider the physical meaning of the parameter f, used in Figs. 2 and 3, and defined by Eq. (1). Substituting (7) and (8) into (5a), one finds directly

$$\frac{\rho_m}{\rho_0}=\frac{\rho-\rho_r(\infty)}{\rho_0-\rho_r(\infty)}\equiv f, \tag{9}$$

which is the same as (1). Thus, f at any time represents the fraction of the initially quenched-in concentration of defects which has still not been annealed out. The curve in Fig. 2 represents the decay of these defects as

[11] S. Yoshida and J. S. Koehler, Acta Met. 8, 878 (1960).

[12] A. Howie, Phil. Mag. 5, 251 (1960).

a function of time, plotted here on dimensionless scales. The universality of this curve indicates that by quenching pure Au from above 800°C the annealing out of the quenched-in defects takes place by one unique process.

VI. THE S-SHAPED CURVE

By summarizing the results of the preceding sections, we can now develop a picture of the life history of supersaturated concentrations of vacancies in Au during the annealing in the neighborhood of room temperature after quenching from above 800°C. We can adjust the general set of equations given in (1) of Paper I to this specific problem and determine the boundary conditions. Finally we try to solve these equations and compare the results with the experimental data.

In Au quenched from above 800°C, single-, di-, and tri-vacancies are in thermal equilibrium with each other (Sec. III). The only other complexes present are tetra- and penta-vacancies, which are so stable that they do not anneal out in the vicinity of room temperature. The single-, di-, and some of the tri-vacancies are mobile (see Paper I) and anneal out by absorption at the stable dislocation network and at the tetrahedra which are formed during the annealing process. The differential equations which govern the kinetics of these vacancies and vacancy clusters are given by Eqs. (1a–g) of Paper I. The boundary conditions are

$$\begin{aligned} c&=0 \quad \text{at } r=b \quad \text{and for} \quad \text{all } t,\\ \partial c/\partial r&=0 \qquad r=R \qquad\quad\ \ \text{all } t,\\ c&=c_0 \quad \text{all } r \qquad\quad\ \ t=0. \end{aligned}$$

Here, b is the radius of the core of the dislocation (and also of the stairrods of the tetrahedra). $2R$ is the average distance between two sinks. $c=c_1+2c_2+3c_3+4c_4+5c_5$.

The first boundary condition should require that the concentration at the dislocation be equal to the equilibrium concentration at the annealing temperature. However, this concentration is so small that we select it to be zero.

One is actually interested in the calculation of ρ_m which is the parameter plotted in Fig. 2 (Sec. V). Taking the time derivative of ρ_m in Eq. (5b) and substituting into it Eqs. (1a–g) of Paper I, one obtains the very simple rate equation for ρ_m:

$$d(\rho_m/\rho_v)/dt=(D_1\nabla^2c_1+2D_2\nabla^2c_2+3D_3{}^d\nabla^2c_3{}^d). \quad (10)$$

The defects anneal out at the dislocation network and at the tetrahedra. That the latter process dominates can be seen as follows: Let n be the number of tetrahedra per unit volume and $2R_t$ their average spacing. Similarly, let d be the density of dislocations with average spacing $2R_d$. The tetrahedra dominate as sinks if $R_t<R_d$, i.e., if $n^{2/3}>d$. For a 900°C quench the final concentration of tetrahedra is $n_\infty\sim10^{15}$ per cc. With $d\sim10^8$ per cm^2 one finds that the condition holds as soon as $n/n_\infty\sim10^{-3}$. We will see below that the time t required to reach this is $t=10^{-3}t_{1/2}$ or about 1 min. We will therefore neglect the annealing out of defects at the dislocation network for *all* times.

We have not been able to integrate the nonlinear ordinary differential equations for the singles and divacancies including their concentration dependence (Paper I). We therefore used the method of Dienes and Damask[13] and neglected this concentration dependence. Thus, one assumes the concentration of each of the defects to be homogeneous throughout the solid including the boundaries of the sinks. If we further assume that the tetrahedra are distributed at random and that interactions between vacancies and tetrahedra are essentially of short range, then (10) can be written as

$$d(\rho_m/\rho_v)/dt=-(D_1c_1+2D_2c_2)m\Gamma n/Na^2, \quad (11)$$

with the boundary condition $\rho_m=\rho_0$ and $n=0$ for $t=0$. We neglected the contribution of the migration of the trivacancy since their concentration is small (see Paper I). m is defined in Sec. IV, Γ is a geometrical factor similar to the preexponential factors in Table I of Paper I ($\Gamma\sim100$). The second boundary condition expresses the assumption that no sinks are present directly after quenching. As mentioned in Sec. III, Cotterill's observations on freshly quenched Au foils are not conclusive. However, the boundary condition is also strongly suggested by our annealing curves, which show that $(d\rho_m/dt)_{t\to0}\to0$ (see Figs. 2 and 3, and especially Fig. 2 of Paper I).

In order to solve Eq. (11) one has to rewrite c_1 and c_2 in terms of ρ_m. c_2 can be eliminated using the equilibrium condition; c_1 can be expressed into ρ_m by means of Eq. (5b). We will neglect the contribution of tri- and tetra-vacancies to ρ_m (for a 900°C quench $3c_3/c_0\sim0.10$ and $4c_4/c_0\sim10^{-2}$). For the trivacancies this approximation is probably too crude in the case of 1000°C quenches, where trivacancies may be more important (see Paper I). We noted above that in this case deviations from the universal S-shaped curve were found (Fig. 3). The divacancy contribution to the second approximation will be neglected. Hence, one can substitute for c_1,

$$c_1=(\rho_m/\rho_v)[1+12(\rho_m/\rho_v)e^{B_2/kT}]^{-1}. \quad (12)$$

In addition the following assumptions will be made:

(1) Single- and di-vacancies are in thermal equilibrium at all times including $t=0$ (the time required to reach equilibrium at 40°C is about 10 sec).

(2) The corners of the tetrahedra are considered as the absorption sites, i.e., $m=4$ (Sec. IV). For the case that the edges act as such, only the final result will be given.

[13] G. J. Dienes and A. C. Damask, Disc. Faraday Soc. **31**, 29 (1962).

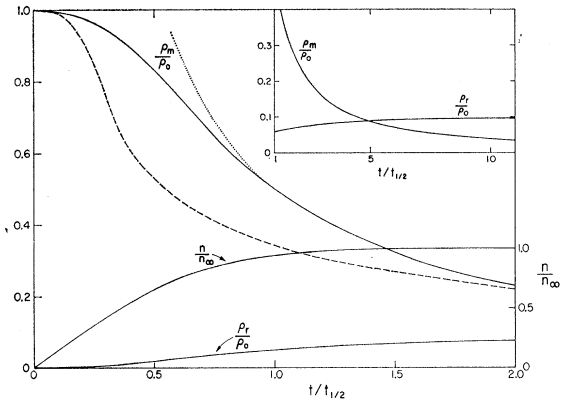

FIG. 9. Calculated curves for ρ_m/ρ_0, ρ_r/ρ_0, and n/n_∞ as a function of $t/t_{\frac{1}{2}}$ (full lines). The dotted line represents the approximation of ρ_m/ρ_0 for long times. The dashed line is the calculated curve of ρ_m/ρ_0 for a model in which the edges of the tetrahedron act as absorption sites instead of the corners.

Introducing the new variable $c_m=\rho_m/\rho_v$, one can write Eq. (11) in the form given in Eq. (13a).

Next, let us examine the rate equation for the formation of the sinks. We mentioned that the tetravacancy is the smallest complex that cannot be annealed out in the vicinity of room temperature; it is converted into a tetrahedron by the encounter with a divacancy (Sec. IV). If we assume that all the tetravacancies formed during the annealing process are struck at least once by a divacancy, then Eq. (1g) represents the rate equation for the formation of the sinks with $dc_4/dt=(1/N)dn/dt$, and the boundary condition $n=0$ for $t=0$. Eq. (1g) can be written in the form (13b) by substituting the equilibrium condition for c_3 and eliminating c_1 as just described. In addition the term ξ can be neglected (Sec. III). Hence,

$$\frac{dc_m}{dt}=-\frac{D_1c_m+(D_1+D_2)pc_m^2}{(1+pc_m)^2}\frac{4\Gamma}{Na^2}n, \qquad (13a)$$

$$dn/dt=\tfrac{2}{3}N\chi_1pe^{B_3/kT}[c_m/(1+pc_m)]^4, \qquad (13b)$$

with $p=12e^{B_2/kT}$; $c_m=c_0$, and $n=0$ for $t=0$.

The set of Eqs. (13) represents the differential form of the S-shaped curve. First we solve them for n as a function of c_m. The number of tetrahedra increase steeply in the beginning (see Fig. 9), and then level off. Therefore in the vicinity of $c_m\sim c_0$, we can replace the denominators by $(1+pc_0)$. In addition one can simplify Eq. (13a) for this situation because $D_1/D_2 \ll pc_0\ll 1$. This means that one neglects the diffusion of singles relative to that of divacancies in the formation of sinks (for a 900°C quench, $pc_0=10^{-1}$ and $D_1/D_2=6\times10^{-2}$). The solution for n is then

$$n=n_\infty[1-(c_m/c_0)^3]^{1/2}, \qquad (14a)$$

with

$$n_\infty=\frac{4\sqrt{2}Nc_0^{1.5}}{\Gamma^{1/2}(1+12c_0e^{B_2/kT})}\times\exp[-(E_m^1-E_m^2-B_3)/2kT], \qquad (14b)$$

where n_∞ is the number of tetrahedra per unit volume at infinite annealing times. Note that one can obtain n as a function of c_m without approximating the denominators. However, the result is complicated and reduces to (14) in the limit.

It follows from (14a) that half of the total number of tetrahedra have formed after 10% of the defects have been annealed out. Examination of (14b) reveals that n_∞ should be proportional with $c_0^{1.5}$. In Fig. 10 a 1.5 power dependence (full line) is compared with Cotterill's data, who determined the concentration of tetrahedra from electron microscopy pictures. His data scatter widely but they are consistent with this prediction. We may also note that n_∞ should be only weakly dependent on temperature since $E_m^1-E_m^2\sim B_3$. This allows us to compare our results obtained by annealing the specimens at 40°C with Cotterill's, annealed at 100°C.

One can calculate the decay of the quenched-in resistivity, ρ_m, as a function of time, $t/t_{1/2}$, by substituting (14a) into (13a) and solving the resulting equation. In this case the complete Eq. (13a) is used including both the diffusion of single vacancies and of divacancies. Although this was not necessary for n because the sinks form before many of the voids have disappeared, it is necessary when calculating c_m because at long times when the total void concentration is low the diffusion occurs by the combined motion of singles and divacancies. The resulting equation was integrated separately for the region $(c_m/c_0)^3\sim1$ and $(c_m/c_0)^3\ll1$ by means of series expansions. The two solutions overlap in the vicinity of $c_m/c_0=0.85$ (for details see Appendix B). Graphs of the thus calculated curves for ρ_m/ρ_0, ρ_r/ρ_0, and n/n_∞ as a function of $t/t_{1/2}$ are presented in Fig. 9. A comparison with the universal S-shaped curve is given in Fig. 2, where the points represent the data for quenches in the range of 845–950°C and the full line is the calculated curve. The agreement between experiment and theory is excellent. We may note in particular the very close fit at long times.

According to this model, the half-time $t_{1/2}$ is given by

$$1/t_{1/2}=3.23\Gamma\nu_2e^{-(E_m^2-B_2)/kT}(n_\infty/N)c_0. \qquad (15)$$

Examination of (14b) and (15) reveals that $1/t_{1/2}$ should be proportional with $c_0^{2.5}$. Figure 11 shows a plot of log $t_{1/2}$ versus logρ_0. The points were obtained from annealing curves similar to Fig. 1, but all carried out on one sample and annealed at the same temperature (40.15±0.02°C). Using the method of least squares one finds a slope of 2.60±0.2, which is in fair agreement with the above prediction.

n_∞ can be evaluated from (15) by substituting the appropriate numbers for the parameters. Using $c_0=2\times10^{-4}$ and $t_{1/2}=1.8$ h (Fig. 11), one finds $n_\infty=3.1\times10^{16}$ per cc, which corresponds with 400 vacancies per tetrahedron. The concentration of tetrahedra thus calculated is considerably higher than Cotterill ob-

served[4] ($n_\infty \sim 10^{15}$ per cc). The difference, however, is probably not too serious because (1) one cannot put too much emphasis on Cotterill's numerical results especially after quenches from very high temperature, (2) we assumed that *all* the tetravacancies will be converted into tetrahedra which tends to overestimate n_∞, and (3) numerical substitution cannot be carried out unambiguously because of the large uncertainties in the pre-exponential factors like Γ and χ which all together can easily give deviations of at least one order of magnitude.

Knowing n_∞ from (15), one can again estimate B_3 from (14b). One finds: $B_3=0.13$ eV, which is in the range suggested in paper I.

Other models were also considered:

(1) Instead of the tetravacancy, the trivacancy may also act as the formation site for the tetrahedra [e.g., Dienes and Damask's tetragonal configuration in Fig. 5(a)]. The resulting curve shows close similarity with the previous one and is identical with it at long times (see also below). A satisfactory agreement with the experimental data of Fig. 2 can be obtained. However, one calculates that $n_\infty \propto c_0$ and $1/t_{1/2} \propto c_0^2$; both powers do not fit the experimental results presented in Figs. 10 and 11. In addition numerical substitution gives that the number of vacancies per sink should be about 5, which is not in agreement with experiment.

(2) Instead of the corners, we assumed that the edges of the tetrahedra are the dominating absorption sites. Then m is given by Eq. (4). The resulting curve is presented as the dotted line in Fig. 9. The time scale has been adjusted such that the results at long times coincide with the previously calculated curves. The shape of the curve is quite different and cannot be fitted with the experimental data of Fig. 2. In addition, we found for this model that $n_\infty \propto c_0^{5/3}$ and $1/t_{1/2} \propto c_0^{2.33}$. The latter power dependence corresponds with a curve in Fig. 11 which is too steep.

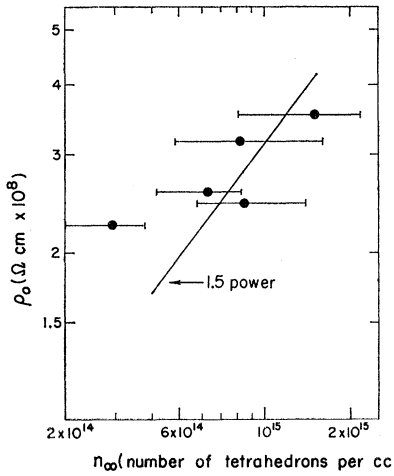

FIG. 10. n_∞ as a function of ρ_0 according to Cotterill's observations (see reference 4). The foils were quenched from above 800°C and annealed at 100°C. The full line represents $n_\infty \propto \rho_0^{1.5}$.

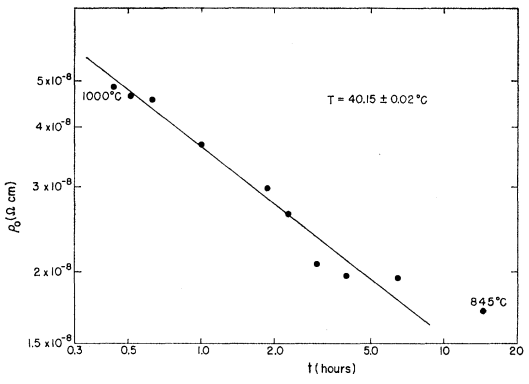

FIG. 11. $t_{\frac{1}{2}}$ as a function of ρ_0 for quenches from above 800°C. The curves from which $t_{1/2}$ was determined were all measured on one sample annealed at one temperature (40.15±0.02°C).

(3) Some models have been considered in which dislocation loops are assumed to act as sinks. In all cases, the curves had the wrong shape, being very similar to the one calculated under (2) (dotted line in Fig. 9).

In all the models investigated, we assumed that the number of absorption sites is proportional with the concentration of sinks and that no sinks are present at $t=0$. In the models under (2) and (3), which resulted in the incorrect curves, it was assumed in addition that the number of absorption sites is proportional with the size of the sink [e.g., application of Eq. (4)]. This latter assumption gave rise to the very steep bend-over in the calculated curves. The physical reason why the latter assumption is incorrect is not yet clear, but is probably related to the interaction between the vacancies and the sinks, about which our knowledge is very rudimentary (see Appendix A).

Equation (13a) also describes the decay of singles and divacancies toward a fixed number of sinks (n=constant). Then Eq. (13a) can be written as

$$dc_m/dt = -(D_1 c_m + D_2 p c_m^2)A, \qquad (16a)$$

with the boundary condition $c_m=c_0$ for $t=0$ and assuming $pc_m \ll 1$. A is a constant containing the concentration of sinks. The solution is

$$\log(c_0/c_m+B) = AD_1 t + \text{const} \qquad (16b)$$

with

$$B=(D_2/D_1)pc_0 \quad (=\tfrac{3}{2}(\nu_2/\nu_1)e^{(E_{m^1}+B_2-E_{m^2})/kT}). \qquad (16c)$$

B actually represents the correction to be applied for the contribution of the migration of divacancies toward sinks [compare with the second term in the numerator of Eq. (3) in Paper I]. Equations (16) can be expected to be a good approximation for the universal curve at long times, where the concentration of sinks can be considered to be constant (Fig. 9). The dotted line in Fig. 9 represents this solution; the curves are identical for $c_m/c_0<0.5$.

Equations (16) are also applicable when singles and divacancies anneal out at the stable dislocation net-

work. For $B\sim1$, divacancies will cause substantial deviations from first-order kinetics. Bauerle[1] observed for quenches from about 700°C first-order annealing kinetics except in the beginning ($0.7<c_m/c_0<1$). Emrick[14] found deviations in the beginning as well as at the tail end, while in addition, in his runs 1.5% of the initially quenched-in resistivity did not anneal out. Figure 12 gives their data plotted according to Eq. (16b), i.e., taking into account divacancies. [Emrick's data are corrected for $\rho_r(\infty)=0.015$ by applying Eq. (1)]. Excellent straight lines can be drawn through Bauerle's and Emrick's points, assuming $B=0.35$ and 1.0, respectively. From B, one can estimate again $E_m{}^1+B_2-E_m{}^2$ by substitution into Eq. (15c). One finds $E_m{}^1+B_2-E_m{}^2=0.245$ and 0.27 eV, respectively, which are consistent with the quoted value of 0.26 ± 0.03 eV reported in Paper I.

VII. SUMMARY

The S-shaped annealing curves observed on Au wires quenched from above 800°C and then annealed in the vicinity of room temperature can be combined into one universal curve by plotting $f=[\rho-\rho_r(\infty)]/[\rho_0-\rho_r(\infty)]$ against the reduced time $t/t_{1/2}$. This universal curve can be understood if one assumes that:

(1) All the quenched-in defects anneal out at tetrahedra of stacking faults which form during the annealing process by the clustering of vacancies.

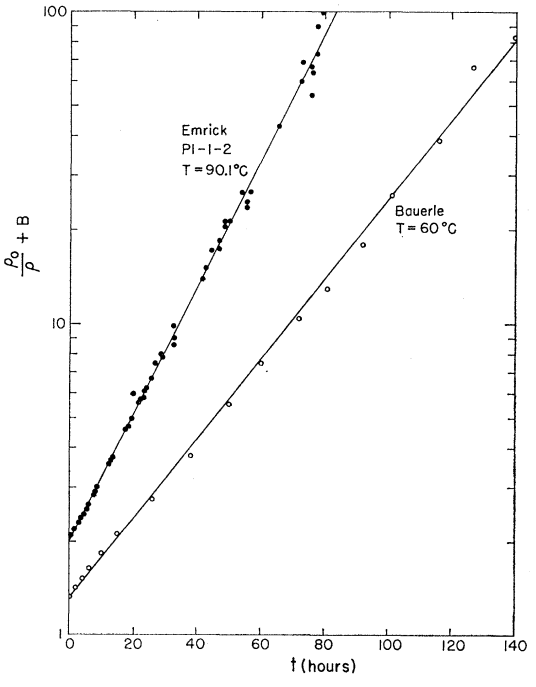

FIG. 12. $\rho_0/\rho+B$ vs time t for Au specimens quenched from 700°C and annealed at 60°C (Bauerle's data, see reference 1) and 90°C (Emrick's data, see reference 14).

[14] R. Emrick, Phys. Rev. 122, 1720 (1961).

(2) Besides the tetrahedra, the other defects present in the crystal are in thermal equilibrium with each other.

(3) The tetravacancies act as the nucleation site for the tetrahedron.

Assumption (1) enabled us to correct the experimental data for the part of the resistivity ρ_r that cannot be annealed out in the vicinity of room temperature (ρ_r is due to the resistivity of the stacking faults) and derive the crucial parameter f, which turns out to represent the fraction of the quenched-in defects that has not yet been absorbed by the tetrahedra.

It is also shown that the tetrahedron can be created by the collapse of six vacancies and therefore will be formed if a tetravacancy is struck by a divacancy, thus making plausible assumption (3). It is observed, and explained from assumption (1) above, that $\rho_r(\infty)/\rho_0$ is independent of the quenching temperature $\rho_r(\infty)/\rho_0=0.74\pm0.006$. The resistivity per unit area of stacking fault in gold is calculated from it to be $\rho_{S.F.}=(1.3\pm0.4)\times10^{-13}$ Ωcm^2.

ACKNOWLEDGMENTS

The authors would like to express their sincere thanks to Dr. A. Serin, who brought the universality of the S-shaped annealing curves to the attention of one of us (J.S.K.); this initiated the present work.

One of us (M.d.J.) is most grateful to Professor D. Lazarus for stimulating and supporting this work, and to the Organization of European Economic Cooperation (O.E.E.C.) for receiving a travel grant which was obtained by the courtesy of the Netherlands Organization for the Advancement of Pure Research (Z.W.O.).

APPENDIX A. THE INTERACTION BETWEEN VACANCIES AND TETRAHEDRA

The interaction between a vacancy and a tetrahedron is very complex. This can be readily seen in a qualitative way. The interaction will be different for the various sites of the tetrahedron, e.g., the corners and the edges, and will be different for singles and divacancies. In addition, the interaction will be strongly direction dependent. Yoshida and Koehler[11] emphasized that divacancies might have, on the average, a larger attractive interaction with dislocations than vacancies because the strain field around a divacancy is larger and has axial rather than cubic symmetry. The magnitude of this interaction depends upon the relative orientation between the dislocation and the divacancy, thus restricting its motion. It is conceivable that the vacancies interact predominantly with the corners of the tetrahedra. The interaction with the faces will be weak because of the low stacking fault energy in Au. The interaction with the dislocations is largely determined by the Burger's vector, which is small for the stairrods ($b=\frac{1}{6}a[101]$).

To make the picture more quantitative, the interaction energy U_d between a divacancy and an edge dislocation is maximal in directions at right angles to the Burger's vector and for an isotropic elastic solid is approximately given by[11,15]

[15] R. W. Cochardt, G. Schoek, and H. Wiedersich, Acta Met. 3, 533 (1955).

$$U_d=[Gba^3/2\pi(1-\nu)](\mathcal{E}/r).$$

G is the modulus of rigidity ($=2.78\times10^{11}$ dyn/cm^2), b is the magnitude of the Burger's vector ($\frac{1}{6}a\sqrt{2}$ for the stairrods), $\mathcal{E}$ is the maximum strain around the divacancy (~0.17), ν is the Poisson's ratio ($=0.45$), and r is the radius between the divacancy and the core of the dislocation. Substituting the numbers in parentheses gives for $r=3a$, $U_d=0.05$ eV. At the corners, the interaction of the divacancy with the three interconnecting dislocations will add in the radial direction (see Fig. 7c) giving $U_c=0.15$ eV and will cancel in the plane at right angles, $U_c=0$.

APPENDIX B

If one neglects the divacancy contribution in (12) and substitutes (14a) into (13a), the differential equation, representing the S-shaped curve, is

$$\frac{dx}{x^2(1+1/ax)(1-x^3)^{1/2}}=-\frac{dt}{\tau}. \tag{B1}$$

Here, $x=c_m/c_0$; $a=12c_0e^{B_2/kT}D_2/D_1$; $1/\tau=1.86/t_{1/2}$ with $t_{1/2}$ given by (15). In our experiments, $a\sim20$. Expansion gives

$$-\frac{dt}{\tau}=\frac{dx}{x^2(1-x^3)^{1/2}}\left[1-\frac{1}{ax}+\frac{1}{(ax)^2}-\frac{1}{(ax)^3}+\cdots\right]. \tag{B2}$$

First consider $x^3\sim1$.

In this region, the series converges very rapidly and only the first term needs to be taken into account. By expansion in powers of $(1-x^3)$ and integration, one obtains

$$\frac{t}{\tau}=\frac{(1-x^3)^{1/2}}{x}+\tfrac{1}{3}(1-x^3)^{1/2}\times\left[1+\frac{1}{9}(1-x^3)+\frac{4}{45}(1-x^3)^2+\cdots\right]. \tag{B3a}$$

Next, consider $x^3\ll1$.

Now all the terms in (B2) have to be included. Expansion of each term in powers of x gives rapid converging series. The result after integration is:

$$\frac{t}{\tau}=\frac{(1-x^3)^{1/2}}{x}+\frac{x^2}{4}[1+\tfrac{2}{5}x^3+\cdots]-\frac{1}{2ax^2}[1-x^3-\tfrac{3}{16}x^6+\cdots]+\frac{1}{3a^2x^3}[1-\tfrac{3}{2}x^3\ln x+\cdots]+\frac{1}{4a^3x^4}[\cdots. \tag{B3b}$$

For $x=1/a$, the solution in this region ($x^3\ll1$) can be given without series expansion by $t/\tau=(1/x)\ln2$. The solutions (B3a) and (B3b) have a common tangent in the vicinity of $x=0.85$. If the divacancy contribution to ρ_m is included in (12), the solutions of the differential equation become more complicated than those presented in (B3) but are essentially similar. The thus calculated curve is given in Fig. 2 and fits the experimental data better in the vicinity of $x=0.80$ than the solutions (B3) but never deviates more from (B3) than by 4%.

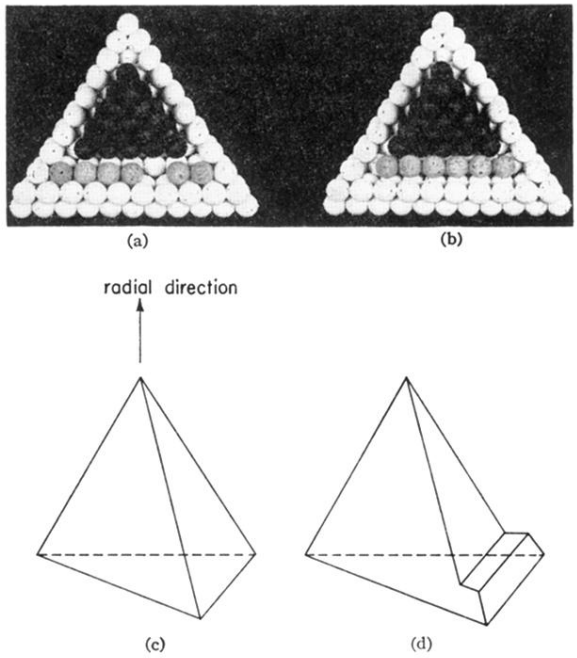

FIG. 7. (a) and (b) Configuration of the atoms adjacent to the edge of a tetrahedron (black balls), before and after absorption of a vacancy (missing atom in the uncolored row of cork balls). (c) and (d) Schematic drawing of the shape of the tetrahedron before and after absorption of a vacancy.